Preparation, Characterization, and Photoelectrochemistry of Langmuir−Blodgett Films of the Endohedral Metallofullerene Dy@C_{82} Mixed with Metallophthalocyanines

Shangfeng Yang, Louzhen Fan, and Shihe Yang*

Department of Chemistry, The Hong Kong University of Science and Technology, Clear Water Bay, Kowloon, Hong Kong

Received: April 24, 2003; In Final Form: June 4, 2003

Stable Langmuir−Blodgett films of the endohedral metallofullerene Dy@C_{82} mixed with metallophthalocyanine (MPc = copper tetra-*tert*-butylphthalocyanine (**1**) and M octakis(octyloxy)phthalocyanine, M = copper (**2**) and zinc (**3**)) are fabricated from the N_2/water interface at a molar ratio of 1:1. Optical, electrochemical, and photoelectrochemical properties of these films have been studied. The packing of Dy@C_{82}/MPc is found to be dependent on the substituents and the central metal ion of MPc, resulting in different relative orientations of the MPc's macrocyclic ring plane and the metallofullerene ball in the Langmuir films. Steady anodic photocurrent responses have been demonstrated for the Dy@C_{82}/MPc mixture films with enhanced quantum yields compared to the pure forms of both MPc and Dy@C_{82}. Dy@C_{82}/**2** (or **3**) are shown to outperform Dy@C_{82}/**1**, giving quantum yields up to 7−8% under appropriate conditions. Both ground-state charge transfer and photoinduced charge transfer between Dy@C_{82} and the octasubstituted MPcs **2** and **3** are proposed. Comparative studies with C_{60} have also been conducted.

Introduction

The success in preparing macroscopic quantities of endohedral metallofullerenes has made it possible to characterize their structures and physical properties during the past few years.[1−5] The encapsulation of the metal atoms in fullerenes brings about many additional, desirable properties such as peculiar redox behavior, radioactivity, luminescence, paramagnetism, and enhanced nonlinear optical response.[6] For example, with the first reduction potentials being even more positive than that of C_{60}, the monometallofullerenes M@C_{82} (M = lanthanide elements) possess a greater electron-accepting ability than C_{60}.[7] This may lead to such applications as photoelectric energy conversion. Previously, we have successfully constructed stable Langmuir−Blodgett (LB) films of the metallofullerene Dy@C_{82} and its mixtures with various molecules such as long-chain arachidic acid (AA).[8,9] The metallofullerene films exhibited a higher photocurrent quantum yield than the corresponding C_{60} films on indium−tin oxide (ITO) electrodes under appropriate conditions.[8] More recently, by incorporating the metallofullerene Dy@C_{82} into a matrix of half-bowl-shaped calix[8]arene, a novel supramolecular complex was prepared, and LB films of this complex have been studied in the context of conformational conversions.[10]

Phthalocyanines (Pcs) and their metalloderivatives (metallophthalocyanines) as porphyrin analogues have attracted increasing interest not only for the preparation of dyes and pigments but also as building blocks for the construction of new molecular materials for electronics and optoelectronics.[11] Octasubstituted or tetrasubstituted Pcs with long alkyl side chains are among the most popular target molecules, largely because of their highly desirable chemical and physical properties. In particular, thin films of Pcs and their mixtures with other molecules are used for applications ranging from chemical sensors, molecular metals, and catalysts to optical storage devices.[12] The LB technique has been an effective technique for the preparation of Pc thin films.[13−20] Considering that Pcs can serve as good electron donors and light-harvesting antenna,[21−25] it would be tempting to construct thin films of new, donor−acceptor-type complexes [Pc−metallofullerene]. This would not only facilitate the film formation but also improve the photoelectric energy conversion properties of metallofullerenes.

SCHEME 1: Molecular Structures of the Three Metallophthalocyanines (MPcs) Employed for the Fabrication of the Mixture Films

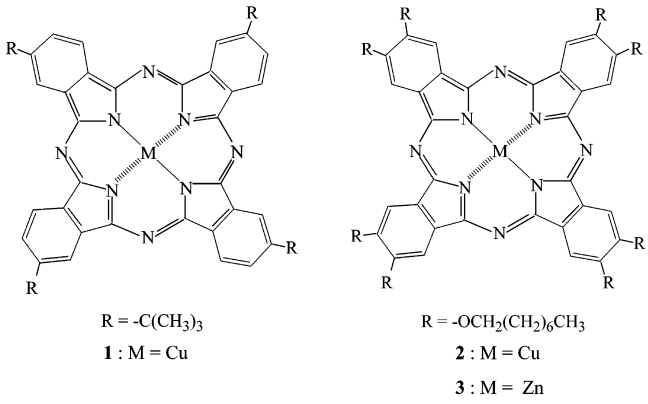

In this paper, we report the preparation, characterization, and photoelectrochemical properties of LB films of Dy@C_{82} mixed with metallophthalocyanine (Dy@C_{82}/MPc). Three different MPcs (**1**−**3**, shown in Scheme 1) are chosen to reveal the effects of the substituents and the central metal on the film structure and property. Dramatic differences in photoelectric response for the different Dy@C_{82}/MPc systems have been observed. Evidence for the ground-state intermolecular charge transfer

* To whom correspondence should be addressed. E-mail: chsyang@ust.hk.

10.1021/jp035107y CCC: $25.00
Published on Web 07/10/2003

(CT) and photoinduced CT has been obtained for the mixture films containing **2** and **3** but not **1**. Experiments with C_{60} have also been done under identical conditions for comparison.

Experimental Section

Materials. High-purity Dy@C_{82} and C_{60} (>99.0%) were prepared by the combination of standard DC arc discharge and HPLC separation.[26−28] The metallophthalocyanines (MPcs) include copper(II) 2,9,16,23-tetra-*tert*-butyl-29*H*,31*H*-phthalocyanine (**1**), copper(II) 2,3,9,10,16,17,23,24-octakis(octyloxy)-29*H*,31*H*-phthalocyanine (**2**), and zinc 2,3,9,10,16,17,23,24-octakis(octyloxy)-29*H*,31*H*-phthalocyanine (**3**) (Aldrich) (see Scheme 1). KCl (Riedel-De Haen AG) was used as electrolyte for photoelectrochemical measurements. L$^{(+)}$-Ascorbic acid (AsA) (Acros Organics Co.) was used as electron donor. Deionized water that had been purified before use by passing through an EASYpure compact ultrapure water system (Barnstead Co.) was used in all of the experiments reported here.

Preparation of LB Films. A Langmuir minitrough (Applied Imaging, U.K.) was employed for the preparation of films. Before experiments, N_2 (purity > 99.99%) was kept flowing for 2 h to minimize the presence of O_2 in the system, which would otherwise cause oxidation and aggregation of the metallofullerene molecules.[9b] The N_2/water interface was thoroughly cleaned by complete barrier movement to ensure that the maximum surface pressure difference was less than 0.2 mN·m^{-1} upon compression. The subphase was ultrapure water (20 ± 1 °C, pH = 6.50, ρ = 18.3 MΩ·cm). The molar ratios of Dy@C_{82}/MPc and C_{60}/MPc (in toluene) were both 1:1 for the spreading solutions with the concentration of (1−2) × 10^{-5} mol·dm^{-3}. A known volume of the Dy@C_{82}/MPc solution (1−2 mL) was carefully spread onto the water surface (505 cm^2) dropwise using a 0.5 mL syringe. This procedure lasted for >1 h. After the solvent evaporated completely (>30 min), the Langmuir films at the N_2/water interface were compressed at a barrier speed of 1 cm/min, and the surface pressure−area (π−A) isotherm was recorded. Monolayer or multilayer LB films of Dy@C_{82}/MPc (or C_{60}/MPc) were deposited from the N_2/water interface by vertical dipping onto a transparent indium−tin oxide (ITO) glass substrate (10 × 15 mm^2, R_s = 85 Ω/□, Delta Technologies Ltd., Stillwater) or quartz plate (10 × 15 mm^2, Electronic Space Products International). The substrates were hydrophilically treated beforehand by refluxing in 2-propanol for 24 h.[29] The LB deposition was carried out at a dipping rate of ∼0.9 mm/min under a constant surface pressure of 15 mN·m^{-1}. A stationary flow of N_2 (∼50 mL/min) was maintained above the water subphase. UV−vis absorption spectra were recorded with a Milton Roy spectrometer (Spectronic 3000). For polarized UV−vis spectroscopy, a polarizer was placed before the sample (see Supporting Information, Figure S1).

Photoelectrochemical Measurements. The photoelectrochemical experiments were performed with a model 600 electrochemical analyzer (CH Instruments Inc.), ITO being the working electrode. A 1000 W xenon lamp (Oriel) was used as the light source. The light intensity was calibrated with a power meter (Newport Co.). Different wavelengths of light ($\Delta\lambda \approx 10$ nm at the exit slit) were obtained with a monochromator (Triax 190, Instruments S. A. Inc.). The electrochemical cell was in a three-electrode configuration, which was under a flowing nitrogen atmosphere to avoid oxygen. Before measurements, the electrolyte solution was bubbled continuously with N_2 (purity > 99.9%) for ∼15 min. The metallofullerene/MPc (or fullerene/MPc) LB films on ITO were used as working electrodes. A Pt wire and Ag/AgCl were used as the counter electrode and the reference electrode, respectively. The electrolyte was an aqueous solution of KCl with a concentration of 0.1 mol·dm^{-3}. For each preparation condition of the LB films on ITO, more than six samples were measured to ensure the reproducibility of the photocurrent data.

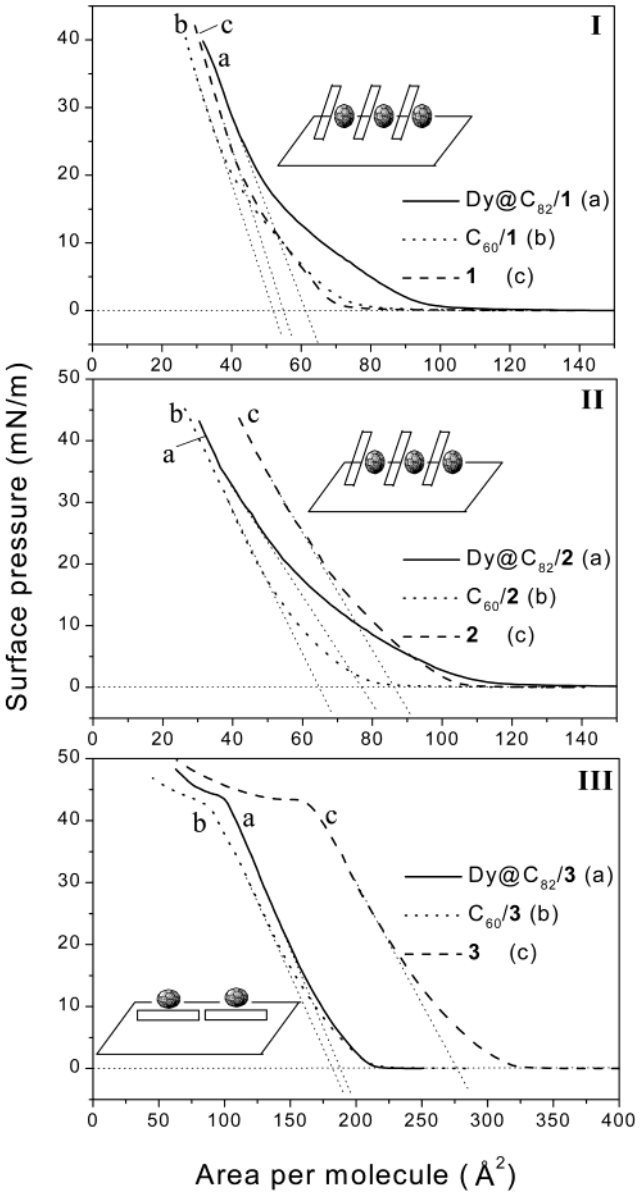

Figure 1. Surface pressure−area (π−A) isotherms of Dy@C_{82}/MPc, C_{60}/MPc, and pure MPc at the N_2/water interface at pH = 6.5: MPc = **1** (I), **2** (II), **3** (III). The barrier compression speed is 2 cm·min^{-1}. The insets illustrate the possible structures of the mixture Langmuir films; the elongated balls are the metallofullerenes and the flat blocks are the MPc molecules.

Results and Discussion

Formation of Langmuir−Blodgett Films. Under our experimental conditions, the metallofullerene/MPc mixtures formed stable Langmuir monolayer films as revealed by the reversibility and reproducibility of the π−A isotherms in the compression−expansion cycles. A typical π−A isotherm of Dy@C_{82}/**1** at the interface between N_2 and ultrapure water at 25 °C is shown in Figure 1 (panel I, line a). The isotherm displays a steep pressure increase in the condensed phase region and no sign of film collapse was observed even when surface pressure reached ∼40

TABLE 1: Characteristics of the Langmuir Monolayers and LB Films Studied in the Present Work

film composition	exptl mean $A_{limiting}$ (Å^2/molecule)	$A_{limiting}$ of Dy@C_{82} or C_{60}[a] (Å^2/molecule)	orientation angle of the MPc ring[b] (deg)	UV−vis absorption peaks (nm)
1	55		36.7	216, 264, 331, 619
Dy@C_{82}/**1**	60	65	61.2	231, 264, 331, 619
C_{60}/**1**	52	49	80.3	221, 269, 341, 619
2	88		48.4	239, 287, 342, 411, 649, 701
Dy@C_{82}/**2**	78	68	54.3	251, 342, 619, 683
C_{60}/**2**	65	42	44.2	221, 268, 342, 619, 683
3	276			241, 350
Dy@C_{82}/**3**	185	*c*		250
C_{60}/**3**	180	*c*		250, 336

[a] The limiting area per molecule (A) of Dy@C_{82} or C_{60} in mixture film (1:1) is calculated as $A = 2A_{mean} - A_{MPc}$, where A_{mean} is the mean limiting area of the mixture film and A_{MPc} is the limiting area of pure MPc. [b] The orientation angle of the MPc ring within the LB film is calculated on the basis of the result of polarized UV−vis absorption spectroscopic characterization (see Supporting Information). [c] Because **3** takes face-on conformation, the method described in footnote a for the calculation of limiting area per molecule (A) of Dy@C_{82} (or C_{60}) in a mixture film is not applicable here.

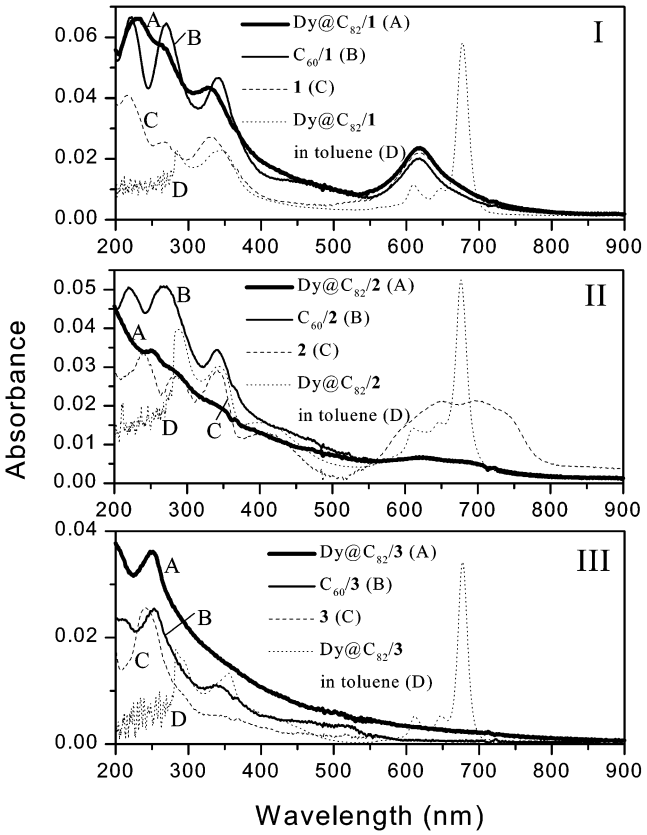

Figure 2. UV−vis absorption spectra of the Dy@C_{82}/MPc, C_{60}/MPc, and pure MPc LB films on quartz plates: MPc = **1** (I), **2** (II), **3** (III). The spectra of the Dy@C_{82}/MPc (1:1) mixture solutions in toluene are also shown as references (dotted lines).

mN·m^{-1}. By extrapolating the condensed phase region of the $\pi-A$ isotherm to zero pressure, the average limiting area per molecule was estimated to be 60 Å^2. For comparison, a $\pi-A$ isotherm of C_{60}/**1** is shown in Figure 1 (panel I, line b), which is similar to that of Dy@C_{82}/**1** except that the average limiting area per molecule is smaller (52 Å^2). All of the isotherm data are summarized in Table 1.

Langmuir film of pure **1** (Figure 1 (panel I, line c)) prepared under the same conditions as those mentioned above gives a limiting area of 55 Å^2. This value is in good agreement with previous reports in which spreading solvents such as benzene, toluene, or chloroform were used, indicating that molecules of **1** take a tilted edge-on conformation with the MPc plane being perpendicular to the interface.[19,20] As a result, Dy@C_{82} or C_{60} molecules might be squeezed into the matrix of the molecules of **1** in the mixed Langmuir films (inset of Figure 1 (panel I)). Furthermore, taking into account the molecular area of **1** (55 Å^2), the molecular area of Dy@C_{82} in Dy@C_{82}/**1** is estimated to be 65 Å^2. This value is larger than that in Dy@C_{82}/AA film (55 Å^2)[8] but still smaller than the minimum cross section of such molecules (e.g., ∼120 Å^2 for Y@C_{82} based on an X-ray diffraction measurement [30]). Similarly, the estimated molecular area of C_{60} is 49 Å^2 in C_{60}/**1** film, which is also smaller than the cross section of free C_{60} (100 Å^2) estimated from X-ray diffraction data.[31a] On the basis of the polarized absorption data described below, the smaller limiting molecular areas estimated above for both Dy@C_{82} and C_{60} are consistent with the fact that the macrocyclic ring planes are much more tilted from the substrate surface than those in the films of pure **1** (see Supporting Information, Table S1).

The $\pi-A$ isotherms of Dy@C_{82}/**2**, C_{60}/**2**, and pure **2** obtained under the same conditions are shown in Figure 1 (panel II, lines a−c). The limiting molecular area of **2** is found to be 88 Å^2, which is significantly larger than that of **1**. This could be explained by the bulky octaalkoxy chains and their suppression of the aggregation of the Pc molecules.[15] However, this area is still much smaller than the area of the Pc ring plane (∼300 Å^2 from a CPK space-filling model),[15a] suggesting that the tilted edge-on conformation is again preferred. Furthermore, from the mean limiting molecular areas of Dy@C_{82}/**2** (78 Å^2) and C_{60}/**2** (65 Å^2), we obtain 68 and 42 Å^2 for the limiting molecular areas of Dy@C_{82} and C_{60}, respectively (see Table 1). Because the complex formation with Dy@C_{82} (or C_{60}), as suggested below, opens up the alkoxy arms of **2**, the actual limiting molecular areas of Dy@C_{82} (or C_{60}) should be larger than the above estimates.

The effect of the central metal on the LB film formation is demonstrated by the use of **3**, as shown in Figure 1 (panel III, line c). With the change of central metal from copper to zinc, the limiting molecular area increases dramatically to 276 Å^2. This is quite close to the Pc ring plane area (∼300 Å^2), indicating the face-on conformation in which the Pc plane is parallel to the interface. In contrast to Cu(II), which prefers square planar coordination, the tetracoordinated Zn(II) in **3** tends to be coordinated by two additional apical OH_2.[18] This prevents the $\pi-\pi$ interactions between the macrocycles and thus favors the face-on packing geometry in the monolayers. As a result of the face-on orientation of **3**, the cage molecules Dy@C_{82} and C_{60} in the mixture films are expected to stand on the macrocyclic ring planes (see inset of Figure 1 (panel III)). In this case, the limiting molecular area is wholly determined by the macrocyclic ring plane of **3** (370 Å^2, see Table 1). This value is much larger than that in the pure **3** film (276 Å^2) presumably because the carbon cage has held open the alkoxy arms of the macrocyclic

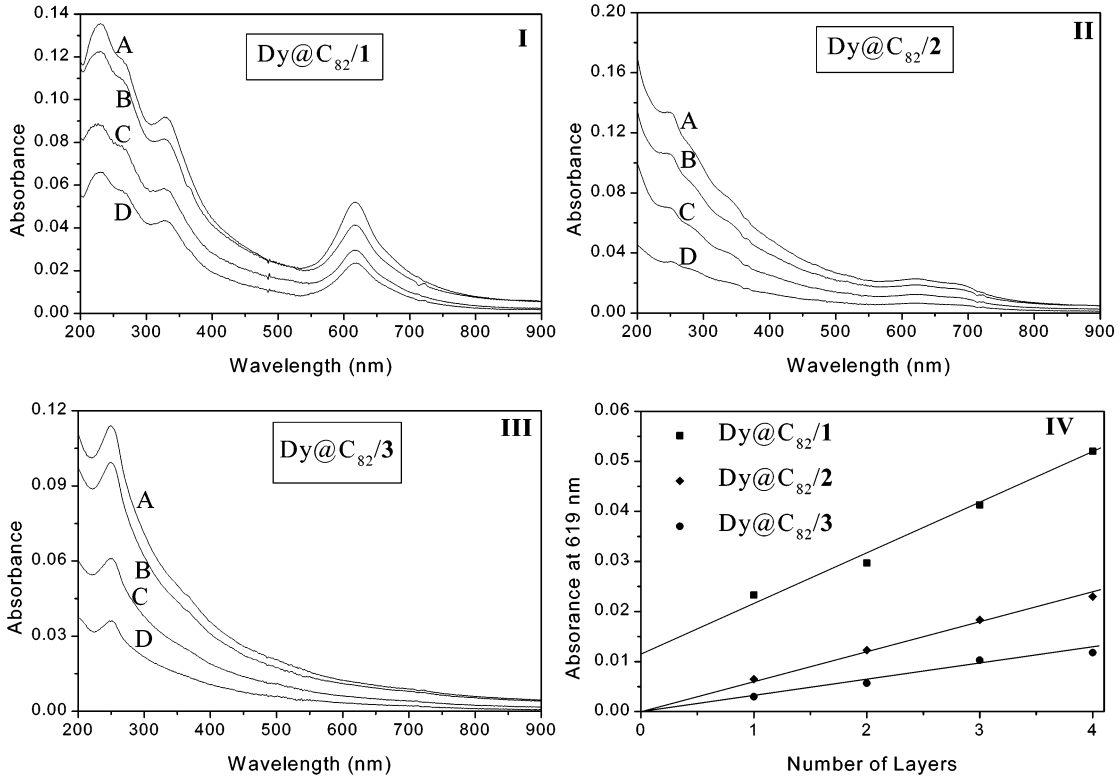

Figure 3. UV−vis absorption spectra of the Dy@C_{82}/MPc LB films on quartz plates as a function of the number of layers (I−III): (A) four layers; (B) three layers; (C) two layers; (D) one layer; MPc = **1** (I), **2** (II), **3** (III). Panel IV shows the absorbance at 619 nm as a function of the number of layers.

ring plane as argued above for fullerene/**2**. An alternative arrangement is that the carbon cages and the MPc molecules are side-by-side in alternation; here, there would be no $\pi-\pi$ interaction.

Absorption Spectra. Monolayer films of Dy@C_{82}/MPc and C_{60}/MPc (MPc = **1**, **2**, or **3**) at the N_2/water interface were transferred onto hydrophilic quartz plates by vertical dipping (upstroke) with a transfer ratio of ∼1, and their UV−vis absorption spectra are shown in Figure 2 (also in Table 1), together with some reference spectra. The spectra of the mixture solutions (D) are simply sums of the spectra of the individual components Dy@C_{82} and MPc. However, the spectra of the LB films are quite different from the corresponding solution spectra. In the film spectrum of **1** (Figure 2, panel I, line C), the Q-band is broadened and blue-shifted to ∼619 nm. The Soret band undergoes the broadening and blue shift (to ∼331 nm) in like manner although to a much less extent. Such spectral features suggest the formation of dimers from the macrocycles.[13b] The spectrum of the Dy@C_{82}/**1** film (Figure 2, panel I, line A) is in general similar to that of the **1** film, except that the Soret band is much stronger than the Q-band due to the modification of Dy@C_{82}. The spectrum of the C_{60}/**1** film follows a similar pattern (see Figure 2, panel I, line B)).

For the **2** film (Figure 2, panel II, line C), the Q-band is significantly broadened (split to two broad peaks at ∼649 and ∼701 nm) and weakened compared to the solution spectrum, but there is not much change in the Soret band (at 342 nm). Here the dimer formation may still take place but to a less extent because the octaalkoxy chains tend to suppress the aggregation of the MPc molecules as mentioned above. The spectra of Dy@C_{82}/**2** (or C_{60}/**2**) films are all the more different. First, the Q-bands are not only much weaker but also further blue-shifted (to 619 and 683 nm; Figure 2, panel II, lines A and B). Second, in the Soret band region, the absorption of Dy@C_{82} and C_{60} becomes more conspicuous than that of **2**.[8,31b] These spectral changes are suggestive of CT from **2** to Dy@C_{82} (or C_{60}) in the film.[23]

By substituting the central metal with zinc, the spectrum of the **3** film (Figure 2, panel III, line C)) becomes totally different from the solution spectrum; the Q-band disappears completely and the Soret band at ∼350 nm is very weak. Such solution-to-film spectral changes are not fully understood, but we also found that **3** exhibits peculiar photochemical properties not shared by **2**.[32] We also prepared LB monolayer films by horizontal transfer and the same spectra were obtained. The incorporation of Dy@C_{82} and C_{60} seems to completely eliminate the Soret band of the **3** film. Judging from the similarity of the spectrum of Dy@C_{82}/**3** to that of Dy@C_{82}/**2**, ground-state CT from **3** to Dy@C_{82} is highly likely.

Polarized electronic absorption spectra of the films of MPcs **1**−**3** and their mixtures with Dy@C_{82} (or C_{60}) have been measured according to the method of Yoneyama et al. (see Supporting Information, Figures S2 and S3).[33] Apparent dichroism at incident angles of 0° and 45° is detected. Using these data, we calculated the orientation angles of the MPc macrocyclic ring planes in different samples, and they are listed in Table 1 (see Supporting Information for details). As can be seen in Table 1, the pure MPcs **1** and **2** are, respectively, oriented at 36.7° and 48.4° with respect to the substrate surface, according with the tilted edge-on conformation of the MPc macrocyclic ring planes deduced from the isotherm data. Because **3** has no detectable Q-band absorption peak, its orientation angle could not be determined by this method. Within the experimental uncertainty (±5%), no significant difference is found for the orientations of MPc in the Dy@C_{82}/MPc and C_{60}/MPc films. It is noticed that the orientation of **2** changes only slightly when it is mixed with Dy@C_{82} (54.3°) and C_{60} (44.2°), whereas there is a large increase in the tilt angle of **1** after mixing with the

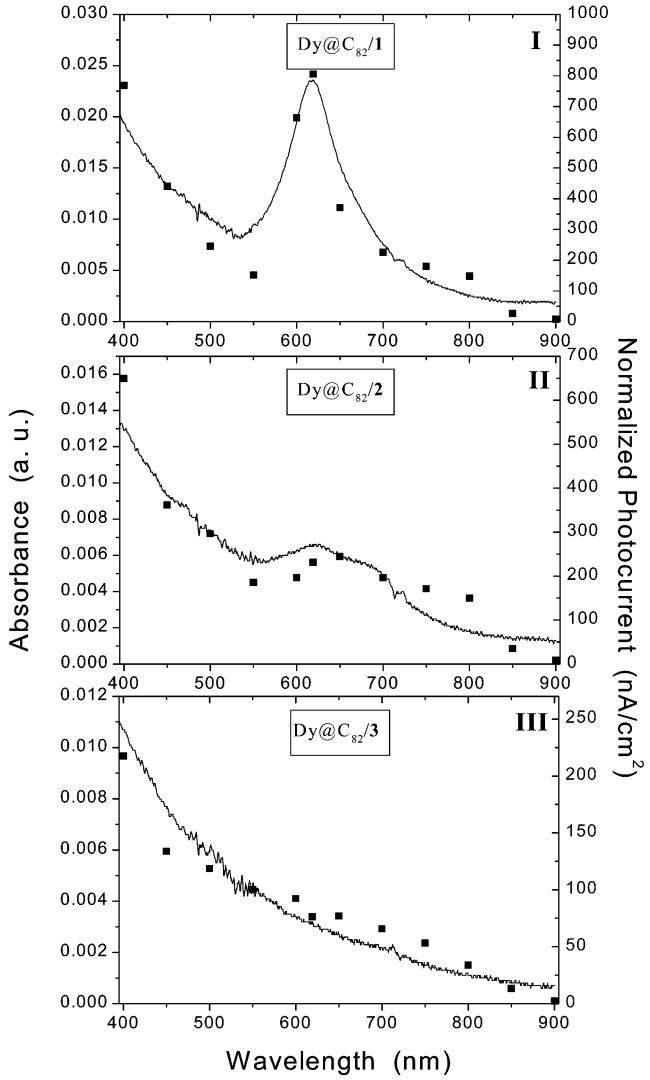

Figure 4. Action spectra (■) of the anodic photocurrents (0.1 mol·dm^{-3} KCl electrolyte solution, 15.0 mmol·dm^{-3} AsA, 0.05 V bias voltage) and absorption spectra (−) for the monolayers of Dy@C_{82}/MPc on ITO (MPc = **1** (I), **2** (II), **3** (III)). The photocurrents are normalized to the incident light intensity at different wavelengths.

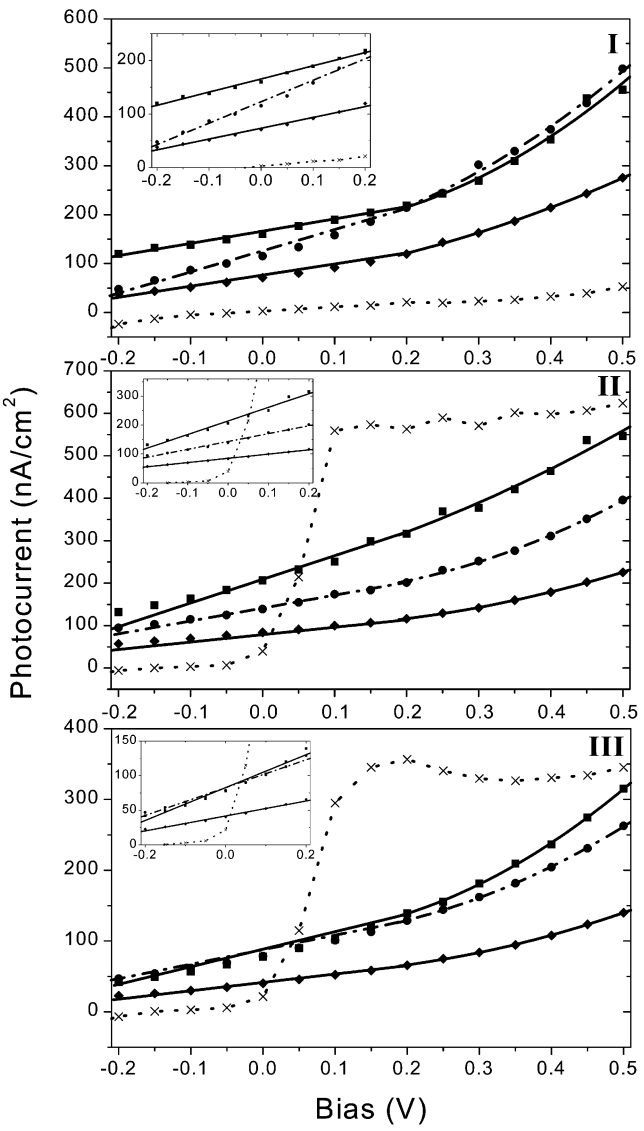

Figure 5. Photocurrent as a function of the electrode potential for the monolayer LB films on ITO (0.1 mol·dm^{-3} KCl electrolyte solution, λ = 550 nm, light intensity = 2.24 mW·cm^{-2}): (■) Dy@C_{82}/MPc; (●) C_{60}/MPc; (♦) pure MPc; (×) dark current of Dy@C_{82}/MPc; MPc = **1** (I), **2** (II), **3** (III). The insets show the linear region from −0.20 to 0.20 V.

fullerenes (60°−80°) (see Supporting Information, Table S1). It appears that the fullerenes disrupt the macrocycle dimer formation from **1**, resulting in an increased tilting. The effect of such disruption, however, becomes less important for **2** because the bulky alkoxy arms have already played the role of curtailing the dimer formation. The fullerene-induced tilting of **1** naturally explains the small limiting molecular areas of the fullerenes estimated above with the isotherm data.

For multilayers of Dy@C_{82}/MPc and C_{60}/MPc, the depositions are found to be of Z-type with the uniform transfer ratio of ∼1 for the upstrokes but nearly zero for the downstrokes. The poor transfer for the downstrokes is presumably due to the hydrophobicity of the molecules, which are not inclined to enter the water subphase.[16,20] Figure 3 (panels I−III) displays the UV−vis absorption spectra of the Dy@C_{82}/MPc LB films on quartz as a function of the number of layers up to four. As the number of layers increases, the absorbance of the LB films increases gradually and the characteristic absorption peaks become more evident. When the absorbance is plotted as a function of the number of layers (Figure 3, panel IV) at 619 nm, linear curves are generally obtained. Perhaps one exception is the Dy@C_{82}/**1** film, for which the absorption of the first layer is higher than those of the subsequent layers. For this film, the structure of the first layer is somehow different from that of the subsequent layers.

Photoelectrochemical Response of the Dy@C_{82}/MPc and C_{60}/MPc Monolayers. Figure 4 shows the photocurrent action spectra for the Dy@C_{82}/MPc monolayers on ITO electrodes along with their absorption spectra (see Supporting Information, Figure S4, for a time trace of the photocurrent response). Because absorption of ITO increases sharply below 340 nm, the photocurrent action spectrum was recorded at wavelengths above 400 nm, where background photocurrent of ITO is negligible. For the three Dy@C_{82}/MPc films studied, the photocurrent spectra coincide well with the corresponding absorption spectra, which strongly suggests that the photoabsorption of Dy@C_{82}/MPc in the LB films is responsible for the photocurrent generation.

Figure 5 shows photocurrent vs bias voltage from −0.20 to 0.50 V (vs Ag/AgCl) for the three MPc systems. The curves consist of two regions, a linear portion in the low-bias region and an exponential rise in the high-bias region. As discussed

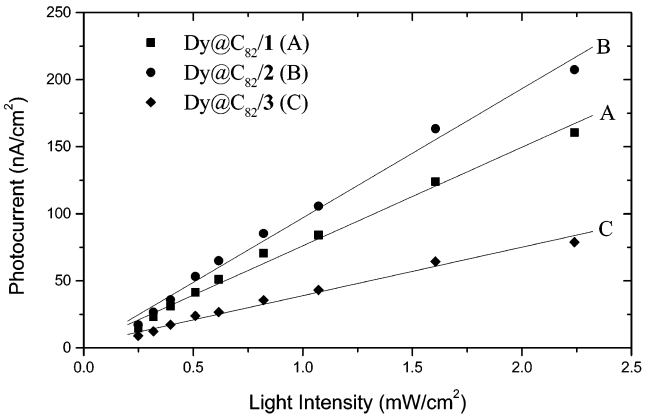

Figure 6. Dependence of photocurrent on light intensity for the monolayer LB films of Dy@C_{82}/MPc (MPc = **1**−**3**, 0.1 mol·dm^{-3} KCl electrolyte solution, no bias voltage, λ = 550 nm): (A) k = 73.49, R = 0.9960; (B) k = 96.23, R = 0.9955; (C) k = 36.12, R = 0.9930. Here, k is slope, and R is correlation coefficient.

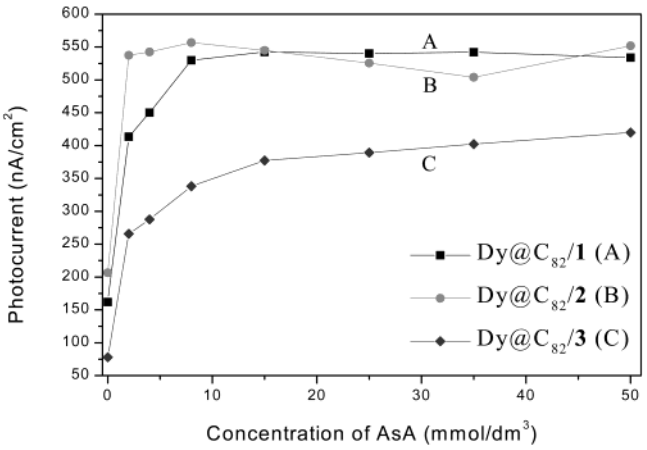

Figure 7. Influence of the ascorbic acid (AsA) concentration on the photocurrent from the monolayer LB films of Dy@C_{82}/MPc on ITO (MPc = **1**−**3**, 0.1 mol·dm^{-3} KCl electrolyte solution, bias voltage = 0.10 V, λ = 550 nm, light intensity = 2.24 mW·cm^{-2}).

previously,[8] two different transport mechanisms appear to be involved for the two bias regions. The first region is due to the film resistance and the second to the space charge effect.[29] Data plotted in Figure 5 also include dark currents as a function of bias voltage. For Dy@C_{82}/**1**, the dark current is much smaller than the photocurrent and increases linearly with the increasing bias voltage from −0.20 to 0.50 V. Dy@C_{82}/**2** and Dy@C_{82}/**3**, however, exhibit quite different $I-V$ characteristics; the anodic dark currents increase sharply with the increasing positive bias on ITO and saturate at ∼0.10 V. The large dark currents in Dy@C_{82}/**2**(**3**) but not Dy@C_{82}/**1** are in line with the inference of the CT complexes [**2**$^+$(**3**$^+$)Dy@C_{82}^-] from the UV−vis spectroscopic data. At a critical positive bias, the electron injection from Dy@C_{82}^- to ITO becomes possible, creating the dark currents. Such dark current surge has also been observed for the C_{60}/**2**(**3**) films but at slightly higher positive bias (∼0.15 V).

The photocurrent response of the Dy@C_{82}/MPc LB films increases linearly with light intensity, as illustrated in Figure 6. In the range of photon fluxes used, no sign of photocurrent saturation was observed. The linearity between the measured photocurrent and light intensity indicates a unimolecular recombination process of separated charges.[34] Noteworthy are the increasing slopes of the photocurrent−light intensity curves from Dy@C_{82}/**3** (C), Dy@C_{82}/**1** (A), to Dy@C_{82}/**2** (B). The different slopes are another indication of the different photocurrent quantum yields for the mixture films, which are clearly dependent on the absorbance and the efficiency of exciton formation, charge separation, and carrier collection.

We have studied the effect of AsA as an electron donor on the photoelectric response. As shown in Figure 7, the anodic photocurrent increases with the increasing AsA concentration. A maximum photoelectric response is reached at an AsA concentration of ∼8 mmol·dm^{-3} for Dy@C_{82}/**1** (A), ∼2 mmol·dm^{-3} for Dy@C_{82}/**2** (B), and ∼15 mmol·dm^{-3} for Dy@C_{82}/**3** (C). The enhancement of the anodic photocurrent by AsA gives a further support of the inference above that the photogenerated electrons flow from the electrolyte through the metallofullerene/MPc monolayer to the ITO substrate. It should be pointed out that the presence of the donor not only boosts the photocurrent but also enhances the dark current of the Dy@C_{82}/MPc monolayer. Furthermore, the photocurrent is attenuated slightly over time, which may be due to the consumption of photoactive molecules during the photocurrent generation processes. Interestingly, after the light and the bias are removed for a brief period of time and then turned on again, the initial photocurrent level is recovered.

TABLE 2: Photocurrent Density (i, nA/cm^2) and Quantum Yields (Φ) of the LB Films of Dy@C_{82}/MPc and C_{60}/MPc on ITO under Different Conditions

	KCl[a]			KCl, AsA, bias[b]				
film	i	A[c]	Φ (%)	i[d]	Φ (%)[d]	i[e]	A[e]	Φ (%)[e]
1	71	0.0064	0.49	275	1.92	583	0.0079	2.64
Dy@C_{82}/**1**	160	0.0095	0.74	635	2.95	2223	0.0194	4.10
C_{60}/**1**	115	0.0073	0.69	474	2.85	1727	0.0155	3.96
2	84	0.0046	0.91	250	2.70	1192	0.0128	3.75
Dy@C_{82}/**2**	207	0.0056	1.64	661	5.20	2610	0.0129	7.21
C_{60}/**2**	139	0.0061	1.13	435	3.55	2016	0.0165	4.94
3	40	0.0015	1.35	104	3.52	370	0.0031	4.86
Dy@C_{82}/**3**	78	0.0047	0.73	496	4.66	1935	0.0107	6.44
C_{60}/**3**	79	0.0016	2.17	212	5.82	1159	0.0051	8.04
Dy@C_{82}/AA[f]	38	0.0041	0.47	156	1.86	521	0.0080	2.57
C_{60}/AA[f]	17	0.0020	0.42	56	1.40	310	0.0065	1.94

[a] Irradiation under 550 nm light of 2.24 mW/cm^2, no AsA, no bias voltage. [b] [AsA] = 15 mM, bias volage = 0.1 V. [c] A = absorbance of LB film at 550 nm. [d] Irradiation under 550 nm light. [e] Irradiation under 400 nm light. A = absorbance of LB film at 400 nm. [f] AA = arachidic acid (refs 8 and 31b).

The external quantum yield is estimated according to $\Phi_\lambda = (I_{ph}/q)/(F_{abs})_\lambda$,[35] $(F_{abs})_\lambda = F_{i\lambda}(1 - 10^{-A_\lambda})$, where I_{ph} is the photocurrent (nA cm^{-2}), q is the elementary charge in coulombs, $F_{i\lambda}$ is the incident photon flux (photons cm^{-2} s^{-1}), and A_λ is the monolayer absorbance at the wavelength λ. The results at 400 nm are tabulated in Table 2. The photocurrent quantum yields of **1**, **2**, and **3** are 2.64%, 3.75%, and 4.86%, respectively. The performance of **3** is noteworthy because its photocurrent quantum efficiency tops those of most organic dyes (0.4−3.6%).[36] After Dy@C_{82} and the MPcs are uniformly mixed, the photocurrent quantum yield goes up significantly. For Dy@C_{82}/**1**, the quantum yield is 4.10%, which is lower than the sum but higher than the mean of the individual contributions. Photoinduced CT between Dy@C_{82} and **1** is believed to play an important role in the photocurrent generation. Even higher quantum yields have been obtained with Dy@C_{82}/**2** (7.21%) and Dy@C_{82}/**3** (6.44%). In this case, ground-state CT between Dy@C_{82} and **2** (**3**) is known to occur. Photoexcitation of the CT complex may further promote the current generation. In fact, photoinduced CT between fullerenes (C_{60} and C_{70}) and tetra-*tert*-butylphthalocyanine (or its zinc derivative) in solution has

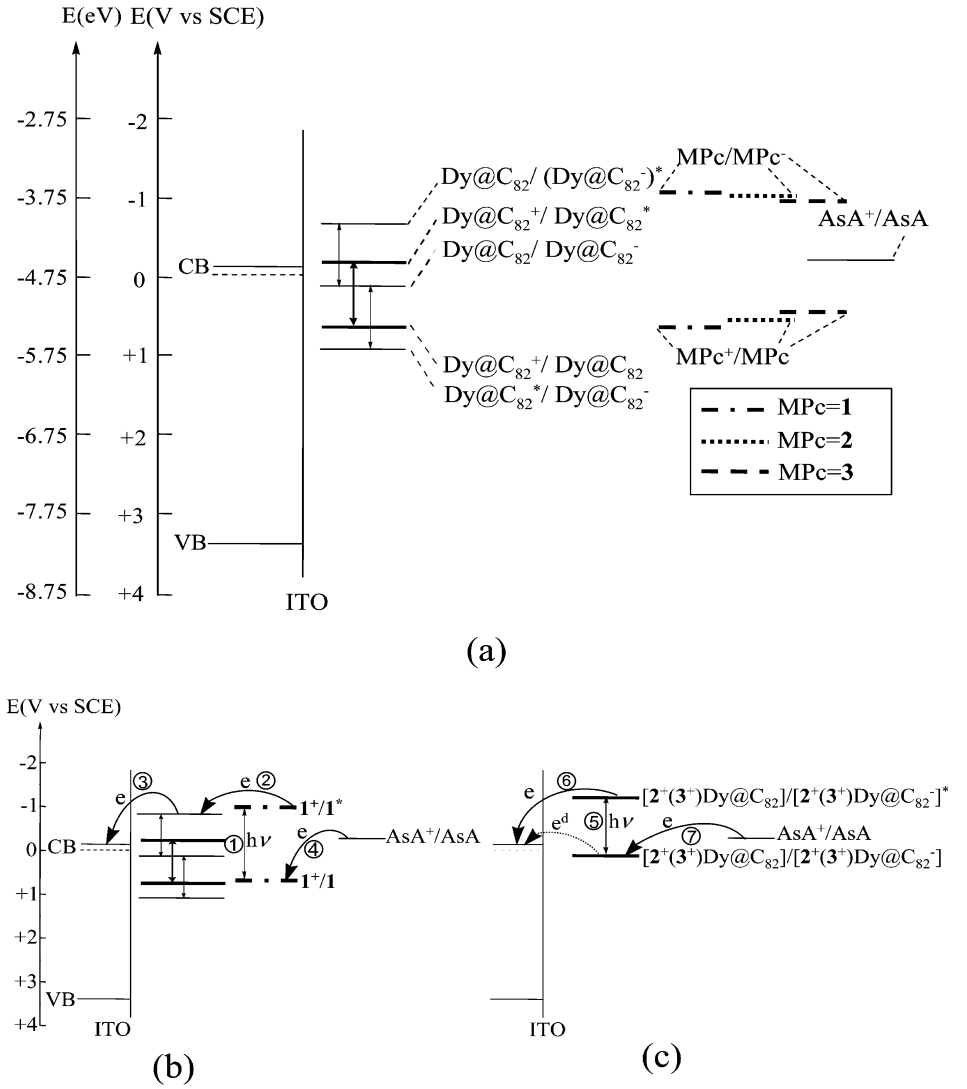

Figure 8. Schematic electron-transfer processes for the anodic photocurrent generation: (a) energy level diagram; (b) possible electron-transfer processes for Dy@C_{82}/**1**; (c) possible electron-transfer processes for Dy@C_{82}/**2**(**3**). e^d denotes the electron-transfer responsible for the dark current.

been confirmed by the nanosecond laser photolysis method.[25] Besides, a CT complexes between C_{60} and an analogue of **2** was thought to be formed in LB films.[22b]

In general, the trends of the photoelectric response for C_{60}/MPcs are similar. Although the photocurrent quantum efficiency of Dy@C_{82}/**2** is higher than that of C_{60}/**2** by ∼50%, C_{60}/**3** exhibits a quantum efficiency as high as 8.04%, which is ∼25% higher than that of Dy@C_{82}/**3**. Such subtle facets are expected to depend on the structural details of the CT complexes.

To probe the energy levels relevant to the photoelectrochemistry, the first reduction potentials and the first oxidation potentials of MPc **1**−**3** are measured both in solution and in LB monolayer film (see Supporting Information, Figure S5). With these results and other available data from literature (Table 3),[7g,8,37−40] a schematic energy level diagram (panel a) and the possible electron-transfer processes (panels b and c) for the ITO/(Dy@C_{82}/MPc)/AsA systems are constructed and shown in Figure 8. It should be mentioned that the reduction and oxidation potentials of the metallofullerene are based on the solution data, and they may be somewhat different in the film states. For the Dy@C_{82}/AA (AA = arachidic acid) system that we studied previously,[8] we proposed that photoexcitation of Dy@C_{82} lead to the direct electron injection to the conduction band (CB) of ITO, forming Dy@C_{82}^+. This state of affairs is relatively simple because AA is neither photo- nor redox active. In the present case, however, MPcs are both good photon grabbers and good electron donors, and this points to different and more intricate photocurrent generation mechanisms. For Dy@C_{82}/**1**, photoexcitation of **1** may result in the electron transfer to Dy@C_{82}, which is then injected to the CB of ITO. A donor such as AsA replenishes the electron ($E^0_{AsA^+/AsA}$ = −0.21 V vs SCE), completing the external circuit. Due to the lower reduction potential of AsA than H_2O ($E^0_{O_2/H_2O}$ = 0.66 V vs SCE at pH = 5.60), an enhancement of the anodic photocurrent is obtained. The overall process runs as follows (see Figure 8b):

TABLE 3: $E^{I/II}$ (V vs SCE)[a] by Cyclic Voltammetry[b] and HOMO−LUMO Gap Energy (E_g, eV) of MPc (1−3) and Dy@C_{82} (C_{60})

compound	$E^{1+/0}$	$E^{0/1-}$	E_g [c]	$E^{1+/*}$ [d]	$E^{*/1-}$ [d]	ref
1	0.69	−1.16	1.60	−0.91	0.44	17a, this work
2	0.55[e]	−1.02[e]	1.60	−1.05	0.58	this work
3	0.48[e]	−0.91[e]	1.60	−1.12	0.69	this work
Dy@C_{82}[f]	0.712	0.213	0.80	−0.088	1.103	7g, 8
C_{60}	1.76	−0.68	1.77	0.01	1.09	31b, 37

[a] $E^{I/II}$ is the reduction potential from state I to state II. [b] In a 0.1 mol·L^{-1} acetonitrile solution of $(n\text{-Bu})_4NPF_6$. Scan rate = 100 mV/s. [c] Estimated from the onset of the UV−vis absorption spectrum. [d] The asterisk (*) denotes the excited state. [e] Irreversible waves (see Supporting Information). [f] Solution data.

$$\mathbf{1} + h\nu \rightarrow \mathbf{1}^* \quad (1)$$

$$\mathbf{1}^* + \mathrm{Dy@C_{82}} \rightarrow \mathbf{1}^+ + \mathrm{Dy@C_{82}}^{-*} \quad (2)$$

$$\mathrm{Dy@C_{82}}^{-*} + \mathrm{CB_{ITO}} \rightarrow \mathrm{Dy@C_{82}} + \mathrm{e^-(CB_{ITO})} \quad (3)$$

$$\mathbf{1}^+ + \mathrm{AsA} \rightarrow \mathbf{1} + \mathrm{AsA}^+ \quad (4)$$

The mixture films containing **2** and **3** are different in that CT has already occurred in the ground state. This is witnessed by a diode-like behavior, that is, a large current surge above a threshold positive bias (Figure 5). Here, the photoexcitation is then on the CT complexes. Once excited, the electron is readily injected into the CB of ITO. Clearly, the excited and injected electron is originally largely localized on the acceptor $Dy@C_{82}$. The following equations summarize the possible photocurrent generation mechanism (see Figure 8c):

$$[\mathbf{2}^+(\mathbf{3}^+)\mathrm{Dy@C_{82}}^-] + h\nu \rightarrow [\mathbf{2}^+(\mathbf{3}^+)\mathrm{Dy@C_{82}}^-]^* \quad (5)$$

$$[\mathbf{2}^+(\mathbf{3}^+)\mathrm{Dy@C_{82}}^-]^* + \mathrm{CB_{ITO}} \rightarrow [\mathbf{2}^+(\mathbf{3}^+)\mathrm{Dy@C_{82}}] + \mathrm{e^-(CB_{ITO})} \quad (6)$$

$$[\mathbf{2}^+(\mathbf{3}^+)\mathrm{Dy@C_{82}}] + \mathrm{AsA} \rightarrow [\mathbf{2}^+(\mathbf{3}^+)\mathrm{Dy@C_{82}}^-] + \mathrm{AsA}^+ \quad (7)$$

Conclusion

We have successfully constructed Langmuir films of the novel donor−acceptor systems $Dy@C_{82}$/MPc (1:1, MPc = **1**−**3**) at the N_2/water interface for the first time. Monolayer and multilayer LB films were deposited on quartz and ITO substrates. The assembly of $Dy@C_{82}$/MPc in the Langmuir films is found to be dependent on the substituents and the central metal ion. Face-on and edge-on geometries for the macrocycles in the films have been inferred with the metallofullerenes sitting on the ring planes for **1**(**2**) and **3**, respectively. Ground-state CT is observed between **2**(**3**) and $Dy@C_{82}$. Stable anodic photocurrent responses for the $Dy@C_{82}$/MPc mixture films have been demonstrated with enhanced quantum yields compared to those of pure $Dy@C_{82}$ and pure MPc. The photocurrent generation is believed to be from either photoinduced CT or photoexcitation of the CT complexes between $Dy@C_{82}$ and the MPcs. The highest photocurrent quantum yield of $Dy@C_{82}$/**2** (or **3**) reaches up to 7−8% under the appropriate conditions. C_{60} has also been employed in this study for comparison. This opens new avenues for the development of novel donor−acceptor complexes with potential applications in optoelectronics and solar energy conversion.

Acknowledgment. This work was supported by RGC and NNSF-RGC grants administered by the UGC of Hong Kong.

Supporting Information Available: Detailed setup and data of the polarized UV−vis absorption experiments (on MPc and $Dy@C_{82}$/MPc), representative photocurrent response curve of $Dy@C_{82}$/MPc, and cyclic voltammograms (CV) of MPcs. This material is available free of charge via the Internet at http://pubs.acs.org.

References and Notes

(1) Johnson, R. D.; de Vries, M. S.; Salem, J.; Bethune, D. S.; Yannoni, C. S.; *Nature* **1992**, *355*, 239.

(2) Rosen, A.; Wastberg, B. *J. Am. Chem. Soc.* **1988**, *110*, 8701.

(3) Laasonen, K.; Andreoni, W.; Parrinello, M. *Science* **1992**, *258*, 1916.

(4) Guo, T.; Smalley, R. E.; Scuseria, G. *J. Chem. Phys.* **1993**, *99*, 352.

(5) (a) Kikuchi, K.; Suzuki, S.; Nakao, Y.; Nakahara, Y.; Wakabayashi, T.; Shiromaru, T.; Saito, K.; Ikemoto, I.; Achiba, Y. *Chem. Phys. Lett.* **1993**, *216*, 67. (b) Miller, B.; Rosamilia, J. M.; Dabbagh, G.; Tycko, R.; Haddon, R. C.; Muller, A. J.; Wilson, W.; Murphy, D. W.; Hebard, A. F. *J. Am. Chem. Soc.* **1991**, *113*, 6291.

(6) (a) Shinohara, H. *Rep. Prog. Phys.* **2000**, *63*, 843 and references therein. (b) Yang, S. H. *Trends Chem. Phys.* **2001**, *9*, 31.

(7) (a) Allemand, P. M.; Koch, A.; Wudl, F.; Rubin, Y.; Diederich, F.; Alvarez, M. M.; Anz, S. J.; Whetten, R. L. *J. Am. Chem. Soc.* **1991**, *113*, 1050. (b) Xie, Q.; Perez-Cordero, E.; Echegoyen, L. *J. Am. Chem. Soc.* **1992**, *114*, 3978. (c) Ohsawa, Y.; Saji, T. *J. Chem. Soc., Chem. Commun.* **1992**, 781. (d) Prato, M.; Suzuki, T.; Wudl, F.; Lucchini, V.; Maggini, M. *J. Am. Chem. Soc.* **1993**, *115*, 7876. (e) Kikuchi, K.; Nakao, Y.; Suzuki, S.; Achiba, Y. *J. Am. Chem. Soc.* **1994**, *116*, 9367. (f) Suzuki, T.; Maruyama, Y.; Akasaka, T.; Ando, W.; Kobayashi, K.; Nagase, S. *J. Am. Chem. Soc.* **1994**, *116*, 1359. (g) Wang, W. L.; Ding, J. Q.; Yang, S. H.; Li, X. Y. *Electrochem. Soc. Proc.* **1997**, *97*−*14*, 417.

(8) Yang, S. F.; Yang, S. H. *J. Phys. Chem. B* **2001**, *105*, 9406.

(9) (a) Huang, H. J.; Yang, S. H. *J. Organomet. Chem.* **2000**, *599*, 42. (b) Huang. H. J.; Yang, S. H. Film Formation Behavior of the Endohedral Metallofullerene $Dy@C_{82}$. In *Amorphous and Nanostructured Carbon*; Robertson, J., Sullivan, J. P., Zhou, O., Allen, T. B., Coll, B. F., Eds.; Materials Research Society: Boston, MA, 2000; Vol. 593, pp 63−68. (c) Li, X. G.; Yang, S. F.; Yang, S. H.; Xu, Y.; Liu, Y. Q.; Zhu, D. B. *Thin Solid Films* **2002**, 231.

(10) Yang, S. F.; Yang, S. H. *Langmuir* **2002**, *18*, 8488.

(11) Leznoff, C. C.; Lever, A. B. P. *Phthalocyanines: Properties and Applications*; VCH publishers: New York, 1989, 1993, 1996; Vols. 1−4.

(12) (a) Thomas, A. L. *Phthalocyanine research and applications*; CRC Press: Boca Raton, FL, 1990. (b) Nalwa, H. S. *Supramolecular Photosensitive and Electroactive Materials*; Academic Press: San Diego, CA, 2001.

(13) (a) Fryer, J. R.; Hann, R. A.; Eyres, B. L. *Nature* **1985**, 382. (b) Hann, R. A.; Gupta, S. K.; Fryer, J. R.; Eyres, B. L. *Thin Solid Films* **1985**, *134*, 35.

(14) Snow, A. W.; Jarvis, N. L. *J. Am. Chem. Soc.* **1984**, *106*, 4706.

(15) (a) Matsuzawa, Y.; Seki, T.; Ichimura, K. *Thin Solid Films* **1997**, *301*, 162. (b) Nakahara, H.; Fukuda, K.; Kinoshita, K.; Nishi, H. *Thin Solid Films* **1989**, *178*, 361.

(16) Emelyanov, Y. L.; Khatko, V. V.; Tomchenko, A. A. *Synth. Met.* **1996**, *79*, 173.

(17) (a) Kokubo, H.; Oyama, Y.; Majima, Y.; Iwamoto, M. *J. Appl. Phys.* **1999**, *86*, 3848. (b) Itoh, E.; Kokubo, H.; Shouriki, S.; Iwamoto, M. *J. Appl. Phys.* **1998**, *83*, 372.

(18) Fouriaux, S.; Armand, F.; Araspin, O.; Ruardel-Teixier, A.; Maya, E. M.; Vazquez, P.; Torres, T. *J. Phys. Chem.* **1996**, *100*, 16984.

(19) Matsuura, T.; Komatsu, T.; Hatta, E.; Shimoyama, Y. *Jpn. J. Appl. Phys.* **2000**, 1821.

(20) (a) Ku, I. H.; Lee, Y. L.; Chang, C. H.; Yang, Y. M.; Maa, J. R. *Colloids Surf. A* **2001**, *191*, 223. (b) Sheu, C. W.; Lin, K. M.; Ku, I. H.; Chang, C. H.; Lee, Y. L.; Yang, Y. M.; Maa, J. R. *Colloids Surf. A* **2002**, *207*, 81. (c) Lee, Y. L.; Chen, Y. C.; Chang, C. H.; Yang, Y. M.; Maa, J. R. *Thin Solid Films* **2000**, *370*, 278.

(21) Hiromitsu, I.; Kaimori, Y.; Ito, T. *Solid State Commun.* **1997**, *104*, 511.

(22) (a) Rikukawa, M.; Furumi, S.; Sanui, K.; Ogara, N. *Synth. Met.* **1997**, *86*, 2281. (b) Tanata, D.; Rikukawa, M.; Sanui, K.; Ogara, N. *Synth. Met.* **1999**, *102*, 1492.

(23) Zhao, Y. L.; Gan, L. B.; Zhou, D. J.; Huang, C. H.; Jiang, J. Z.; Liu, W. *Solid State Commun.* **1998**, *106*, 43.

(24) Ding, H.; Ram, M. K.; Zheng, L.; Nicolini, C. *J. Mater. Sci.* **2001**, *36*, 5423.

(25) Nojiri, T.; Alam, M. M.; Konami, H.; Watanable, A.; Ito, O. *J. Phys. Chem. A* **1997**, *101*, 7943.

(26) Ding, J. Q.; Yang, S. H. *Chem. Mater.* **1996**, *8*, 2824.

(27) (a) Ding, J. Q.; Weng, L. T.; Yang, S. H. *J. Phys. Chem.* **1996**, *100*, 11120. (b) Ding, J. Q.; Yang, S. H. *Angew. Chem., Int. Ed. Engl.* **1996**, *35*, 2234.

(28) (a) Huang, H. J.; Yang, S. H. *J. Phys. Chem. B* **1998**, *102*, 10196. (b) Gu, G.; Huang, H. J.; Yang, S. H.; Yu, P.; Fu, J.; Wong, G. K. L.; Wan, X.; Dong, J.; Du, Y. *Chem. Phys. Lett.* **1998**, *289*, 167.

(29) (a) Petty, M. C. *Langmuir−Blodgett Films: Characterization and Properties*; Roberts, G. G., Ed.; Plenum Press: New York, 1990; p 167. (b) Petty, M. C. *Langmuir−Blodgett Films: An Introduction*; Cambridge University Press: Cambridge, U.K., 1996.

(30) Takata, M.; Umeda, B.; Nishibori, E.; Sakata, M.; Saito, Y.; Ohno, M.; Shinohara, H. *Nature* **1995**, *377*, 46.

(31) (a) Kratschmer, W.; Lamb, L. D.; Fostiropolous, K.; Huffman, D. R. *Nature* **1990**, *347*, 354. (b) Luo, C. P.; Huang, C. H.; Gan, L. B.; Zhou, D. J.; Xia, W. S.; Zhuang, Q. K.; Zhao, Y. L.; Huang, Y. *J. Phys. Chem.* **1996**, *100*, 16685.

(32) Yang, S. F.; Yang, S. H. Unpublished results.

(33) Yoneyama, M.; Sugi, M.; Saito, M.; Ikegami, K.; Kuroda, S.; Iizima, S. *Jpn. J. Appl. Phys.* **1986**, 961.

(34) Donovan, K. J.; Sudiwala, R. V.; Wilson, E. G. *Mol. Cryst. Liq. Cryst.* **1991**, *194*, 337.

(35) Miyasaka, T.; Watanabe, T.; Fujishima, A.; Honda, K. *J. Am. Chem. Soc.* **1978**, *100*, 6657.

(36) Zheng, J.; Wu, D. G.; Zhai, J.; Huang, C. H.; Pei, W. W.; Gao, X. C. *Phys. Chem. Chem. Phys.* **1999**, *1*, 2345.

(37) (a) Zhang, W.; Gan, L. B.; Huang, C. H. *Synth. Met.* **1998**, *96*, 223. (b) Zhang, W.; Gan, L. B.; Huang, C. H. *J. Mater. Chem.* **1998**, *8*, 1731. (c) Huang, Y. Y.; Gan, L. B.; Huang, C. H.; Meng, F. *Supramol. Sci.* **1998**, *5*, 457. (d) Zhang, W.; Shi, Y. R.; Gan, L. B.; Huang, C. H.; Luo, H. X.; Wu, D. G.; Li, N. Q. *J. Phys. Chem. B* **1999**, *103*, 675. (e) Wei, T. X.; Shi, Y. R.; Zhai, J.; Gan, L. B.; Huang, C. H.; Liu, T. T.; Ying, L. M.; Luo, G. B.; Zhao, X. S. *Chem. Phys. Lett.* **2000**, *319*, 7.

(38) Ding, J. Q.; Yang, S. H. *J. Phys. Chem. Solids* **1997**, *58*, 1661.

(39) Lin, N. Ph.D. Thesis, The Hong Kong University of Science and Technology, Hong Kong, China, 1997.

(40) Fromherz, F.; Arden, W. *J. Am. Chem. Soc.* **1980**, *102*, 6211.